Pergamon

Int. J. Heat Mass Transfer. Vol. 37, No. 18, pp. 2935–2946, 1994

0017–9310/94 $7.00 + 0.00

0017–9310(94)00115–4

Measurement of opposing heated line jets discharged at an angle to a confined crossflow

Y. R. CHANG and K. S. CHEN†

Department of Mechanical Engineering, National Sun Yat-Sen University, Kaohsiung, Taiwan, R.O.C.

(*Received* 6 *January* 1994 *and in final form* 17 *March* 1994)

Abstract—An experimental study is presented for the discharging of opposing heated line jets at an angle to a confined crossflow. Parametric variations characterizing the mixing processes such as the velocity and temperature trajectories, and the circulation length, are correlated in terms of the momentum flux ratio, the incident angle, and the downstream distance. Measurements show that the turbulence level is high within the region where the mean velocity gradient is steep, and the vertical temperature profiles can be expressed in self-similar forms. Better thermal mixing can be achieved at higher momentum flux ratio and incident angle.

INTRODUCTION

The phenomenon of jets discharged normally or at an angle to a crossflow occurs in various applications. These include the effluent dispersion operation in the industrial processes where streams are mixed for dilution, heat exchange or chemical reaction. For the design considerations in the dilution zone of a gas turbine combustor, the efficient mixing of the diluent air with the high-temperature combustion gases leaving the primary zone is desired to provide a rapid quenching for any ongoing chemical reaction and a more uniform temperature pattern at the turbine inlet [1]. Further, if efficient mixing in the dilution zone can be achieved at a shorter distance, then the size and cost of the combustion chamber can be significantly reduced.

Extensive research has been done on the mixing processes of a single heated jet injected into a cold crossflow [2–5] and of multiple cool jets injected into a heated crossflow [6–10]. These studies provided detailed correlations for predicting the temperature distributions and relevant parametric variations downstream of the jets injected normally from one side into the cold or hot crossflow. Recently, Chen and Hwang [11] investigated the mixing of heated jets injected normally from two sides into a cold crossflow, in which detailed velocity measurements were made.

Most of the previous work is focused on jets discharged *normally* into a horizontal crossflow. However, in certain situations, especially in gas turbine combustors, the diluent air does not enter the combustion chamber perpendicularly through the liner holes, but at an angle with respect to the liner wall of around 60–75° [1, 12]. However, to the authors' knowledge, no experimental data are available that could be used for predicting dual-side configurations taking into account the incident angle.

This paper presents an experimental investigation into the effect of the jet incident angle on the mixing of opposing heated line jets with a horizontal crossflow in a rectangular channel. The objective of this study is to quantify the parametric variations characterizing the mixing of opposing heated line jets with the crossflow. Moreover, the indispensable data base of the mean velocity, turbulence, and temperature for the numerical simulation and turbulence modeling are provided. Detailed velocity and temperature measurements were made by LDV (laser-Doppler velocimetry) and thermocouple probes. Flow visualization by dye injection was also performed. Correlations of mixing characteristics such as the jet velocity and temperature trajectories, the jet half-width, the circulation depth, and the reattachment point in terms of the momentum flux ratio, the downstream distance, and the incident angle, are presented and discussed.

TEST APPARATUS AND PROCEDURES

The main parts of the test facility consisted of one rectangular channel, two identical ducts with heating coils and nozzles for the heated line jets, three air blowers (one for ambient air crossflow, two for heated air jets), and one power control panel, as shown in

† Current address: Institute of Environmental Engineering, National Sun Yat-Sen University, Kaohsiung, Taiwan, R.O.C.

NOMENCLATURE

B	channel width [mm]
D	jet nozzle width (Fig. 3) [mm]
H	channel height (Fig. 3) [mm]
J	momentum flux ratio, $\rho_j V_j^2/\rho_\infty U_\infty^2$
$\bar{T}$	mean temperature [°C]
T_j	mean jet temperature at the nozzle opening [°C]
T_∞	mainstream or crossflow inlet temperature [°C]
U_∞	mainstream or crossflow inlet velocity [in m s^{-1}]
$\bar{U}$	mean horizontal velocity [m s^{-1}]
$\tilde{U}$	velocity difference ratio defined in equation (1)
$\overline{u'}$	root-mean-square component of horizontal turbulent velocity [m s^{-1}]
V_j	mean jet velocity at the nozzle opening [m s^{-1}]
$\overline{v_j'}$	mean jet turbulent velocity at the nozzle opening [m s^{-1}]
$W_{1/2}^{\pm}$	plus or minus jet half-width (Fig. 3)
X	horizontal coordinate
X_R	reattachment point or length of circulation zone (Fig. 3)
Y	vertical coordinate
Y_C	velocity zero-crossing point or jet circulation depth (Fig. 3)
Y_T	jet thermal penetration depth (Fig. 3)
Y_V	jet velocity penetration depth (Fig. 3)
Z	spanwise direction.

Greek symbols

α	jet incident angle relative to the horizontal direction
θ	temperature difference ratio defined in equation (2)
ρ_∞	density of mainstream or crossflow at inlet
ρ_j	jet density at nozzle opening
σ	percentage root-mean-square deviation.

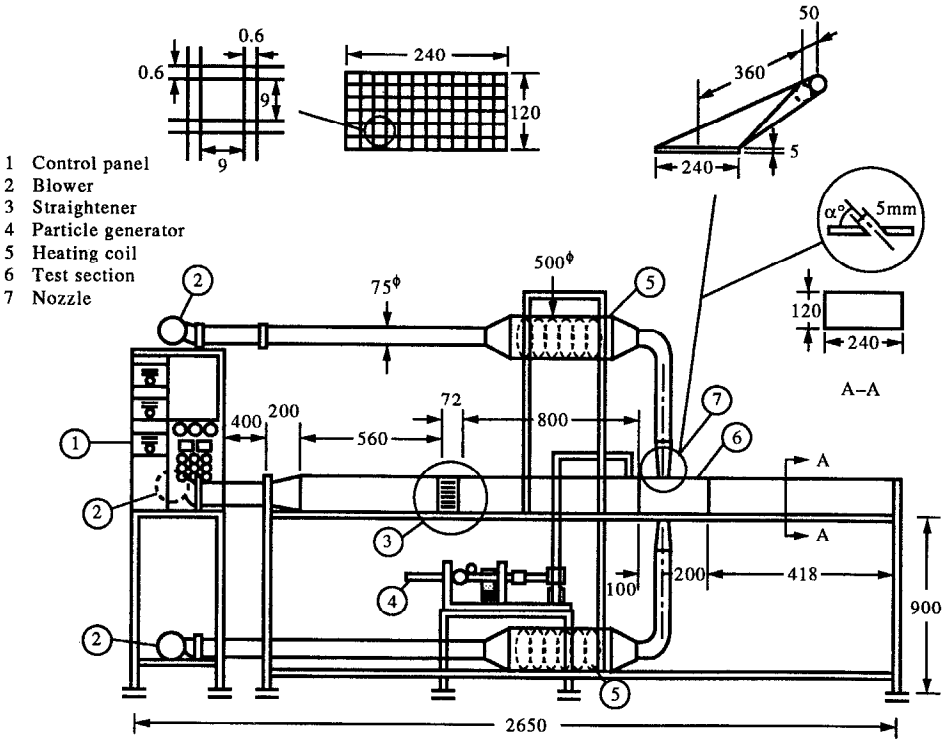

Fig. 1. Schematic of test apparatus (dimensions in mm).

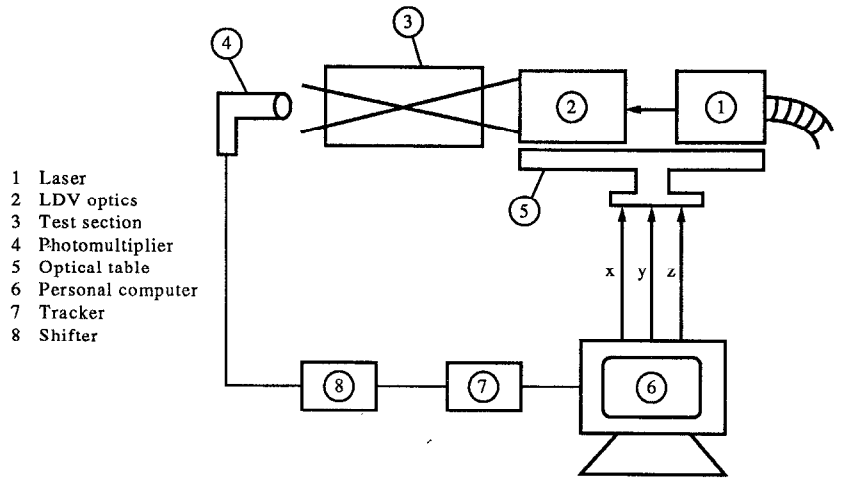

Fig. 2. Sketch of optical system and test apparatus.

Fig. 1. To eliminate the heat losses, the test section and channel walls were covered by 2-cm-thick fine fiberglass insulating material. As shown in Fig. 1, the nozzle was wedge-shaped, 360 mm long from the duct connection and 75 mm in diameter, and expanded to a nozzle opening 240 mm in width. To ensure a two-dimensional flow field at the nozzle exit, the nozzle port was made of a rectangular slot 240 mm in length, 5 mm in width, and 50 mm in depth, that is, the aspect ratio of the nozzle opening is 48 (= 240/5), and the issuing flow is parallel to the opening wall of the nozzle. Both nozzles were in-line and flush-mounted on the top and bottom walls of the channel; and the incident angle α is the jet incident angle relative to the horizontal direction.

The arrangement of the LDV optics and test apparatus, as shown in Fig. 2, is basically similar to that described in Chen and Hwang [11] and Chen and Chang [12]. Consequently, only brief summaries are given below. Measurements of the mean velocity and turbulence components in the horizontal direction were made with a one-component LDV system operating in a forward-scattering, dual-beam mode. The LDV optics include a Spectra-Physics 3W argon-ion laser (green light), a Dantec 55X-series one-color optical assembly (with a 40-MHz Bragg cell), a frequency counter, a frequency shifter, and an RCA photomultiplier. The laser and the optical components were mounted on an optical table, which was equipped with X-, Y-, Z-traversing mechanisms. The movement of the table in each direction was controlled by an ac motor, which was interfaced to a 16-bit personal computer for data acquisition, storage and reduction. A 600-mm focus length achromat formed the probe volume with a waist diameter of approximately 0.1 mm. The light scattered from atomized particles of a glycerol–water mixture with a nominal 1.0 μm diameter was collected by the photomultiplier and subsequently downmixed by the frequency shifter. Calibration of the LDV system was performed by comparing the output signal recorded from a stationary scatter with that obtained directly from the differential signal of the optical–electronic shifter. These calibrations were typically in agreement to within 5 Hz, corresponding to a velocity of about 10 μm s^{-1}. A minimum of 1000 frequency samples were recorded for each measurement from which the mean velocity and turbulent component were calculated by the ensemble average. The nearest distance of the LDV probe volume was about 1.5 mm from the channel wall.

Average temperatures of the flow were measured by Omega Type-T thermocouple wires 2 mm in diameter, of which 12 were mounted equally spaced on a rake. The rake was made of a 120-mm-high aluminum plate with a wing cross-section of 72-mm chord length and 14-mm thickness, and was placed against the top and bottom walls in the channel. All thermocouple wires were connected to a YEW 3088 data logger with automatic ambient compensation. Calibration of the thermocouple wires in a well-mixed ice bed and boiling water showed a maximum error of about ± 0.3°C.

Flow visualization was done by injecting the smoke of the burning incense into the flow. The injector was placed against the top and bottom wall inside the channel at a location about 400 mm upstream of the test section. A 500-W slide projector was used as a light source. Light was shone into the flow from the channel exit. A piece of black paper was placed in front of the light source to form a light sheet. Snapshots were taken with Konica TMAX-400 films at 0.1-s exposure time for most cases.

All measurements of the velocity and temperature of the flow were made on the central plane ($Z = 0$) of the channel in the spanwise direction. The origin O is placed at the bottom and in the central plane of the nozzle opening. The coordinate system and relevant parameters characterizing the mixing processes of thermal and velocity fields are depicted in Fig. 3(a)–(c). In Fig. 3(b), the 'minus' sign (such as $W^{-}_{1/2}$) denotes the quantity near the jet side; while the 'plus' sign (such as $W^{+}_{1/2}$) denotes that away from the jet

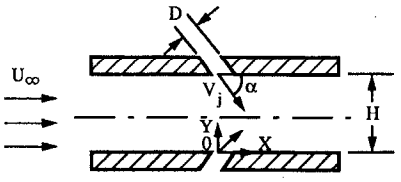

(a) Coordinate system

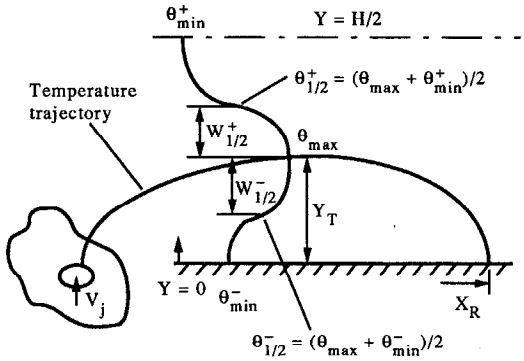

(b) Thermal field

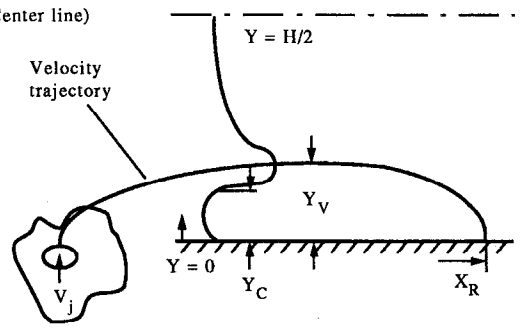

(c) Velocity field

Fig. 3. Coordinate system and relevant parameters characterizing the vertical temperature and velocity profiles.

side. The experimental conditions for the velocity and temperature measurements covered the following ranges:

$$2 \leqslant X/D \leqslant 15$$

$$2.9 \leqslant V_j/U_\infty \leqslant 12.1$$

$$1.123 \leqslant T_j/T_\infty \leqslant 1.127$$

$$0.887 \leqslant \rho_j/\rho_\infty \leqslant 0.89$$

$$7.5 \leqslant J \leqslant 130$$

$$60° \leqslant \alpha \leqslant 90°.$$

The inlet conditions of the crossflow were measured at the upstream location where $X/D = -30$. The typical inlet turbulence level for the crossflow was about 0.7%, and was about 6.5 mm thick (or $6.5 \times 2/120 = 11\%$) for the wall boundary layer when $J = 100$. The typical turbulence level at the nozzle opening was about 3%. It was found that the variations in the velocity and temperature profiles from their mean values at the channel inlet or nozzle opening were within 3.1%.

In the data reduction, only the independent variables of the momentum flux ratio J, the downstream distance X/D, and the incident angle α are considered. The velocity and temperature data are normalized as the difference ratios relative to their associated inlet conditions according to

$$\tilde{U} = \frac{\bar{U} - U_\infty}{\bar{U}_{max} - U_\infty} \quad (1)$$

$$\theta = \frac{\bar{T} - T_\infty}{T_j - T_\infty} \quad (2)$$

where $\bar{U}$ and $\bar{T}$ are the average velocity and temperature at the measured location, and $\bar{U}_{max}$ is the maximum velocity for a given cross section.

RESULTS AND DISCUSSION

Velocity field

Typical mean vertical velocity profiles for various cross sections are shown in Figs. 4 and 5 for $J = 100$, $\alpha = 60°$, and $J = 100$, $\alpha = 75°$, respectively. Figs 4 and 5 show that the velocity profile for each cross section is almost symmetric (within the experimental uncertainties) about the channel mid-height where $Y/H = 0.5$, and, thus, only the lower halves of the velocity profiles are examined.

Figures 4 and 5 also show that the velocity difference ratio $\tilde{U}$ [defined in equation (1)] is negative near the wall-side shear layer; that is, the horizontal velocity of the mixing air is smaller than U_∞ and exhibits a circulation zone near the downstream region of the jet opening. Accordingly, the velocity profile for every cross section has a zero-crossing point, Y_o, at which $\tilde{U}$ changes from a negative to a positive value. For at

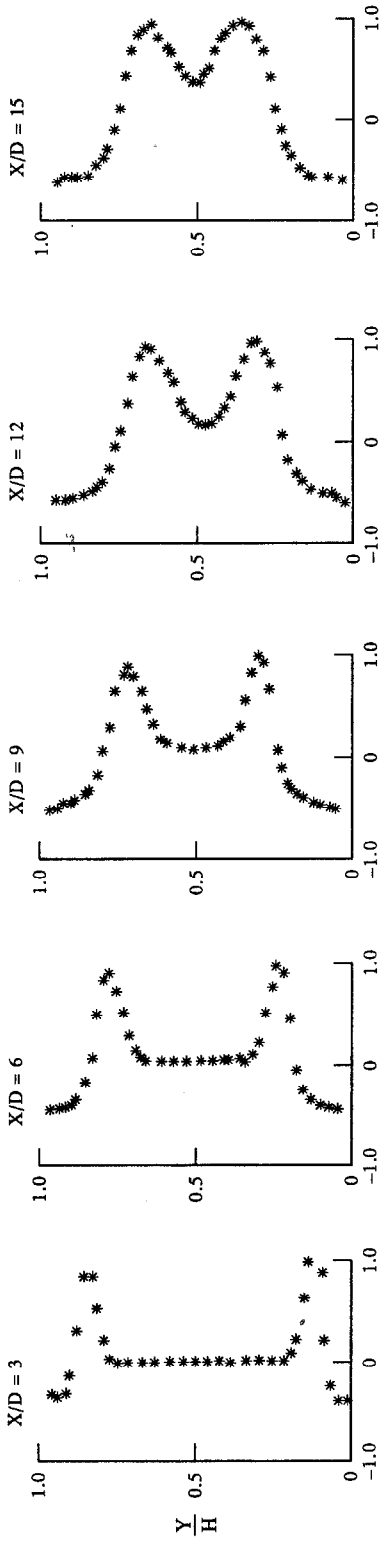

Fig. 4. Vertical velocity profiles at $J = 100$ and $\alpha = 60°$.

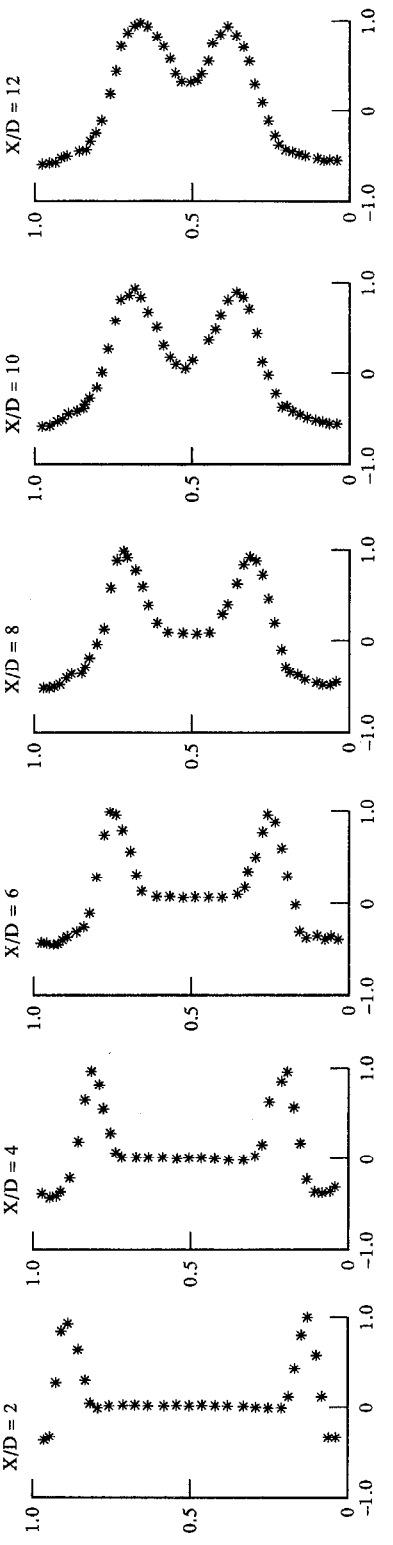

Fig. 5. Vertical velocity profiles at $J = 100$ and $\alpha = 75°$.

Table 1. Correlation equations for opposing line jets

Y_T/D	$\frac{1.372J^{0.257}(X/D)^{0.393}(\sin\alpha)^{4.48}}{1-e^{-C^+}}$	$\sigma = \pm 18.55\%$
$\theta^+_{min}/\theta_{max}$	$C^+ = 0.0043J^{0.273}(X/D)^{0.912}(\sin\alpha)^{6.673}$	$\sigma = \pm 19.76\%$
$\theta^-_{min}/\theta_{max}$	$C^- = 1.570J^{-0.195}(X/D)^{0.375}(\sin\alpha)^{-0.679}$	$\sigma = \pm 22.51\%$
$W^+_{1/2}/D$	$0.723J^{0.125}(X/D)^{0.373}(\sin\alpha)^{0.292}$	$\sigma = \pm 23.12\%$
$W^-_{1/2}/D$	$0.600J^{0.209}(X/D)^{0.19}(\sin\alpha)^{3.267}$	$\sigma = \pm 24.51\%$
X_R/D	$12.23J^{0.225}(\sin\alpha)^{1.99}$	$\sigma = \pm 1.76\%$
Y_v/D	$1.907J^{0.167}(X/D)^{0.427}(\sin\alpha)^{2.42}$	$\sigma = \pm 8.47\%$
Y_c/D	$1.005J^{0.183}(X/D)^{0.477}(\sin\alpha)^{2.474}$	$\sigma = \pm 16.39\%$

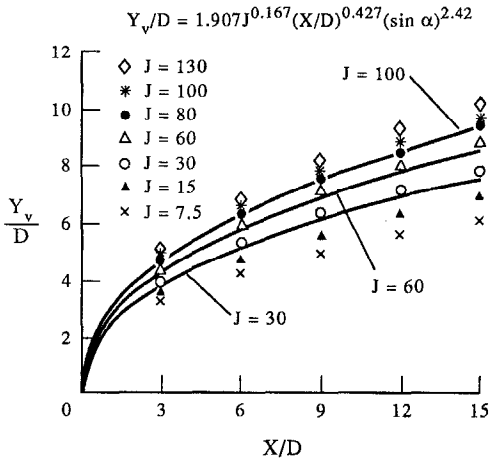

Fig. 6. Correlations of jet velocity trajectory at $\alpha = 60°$.

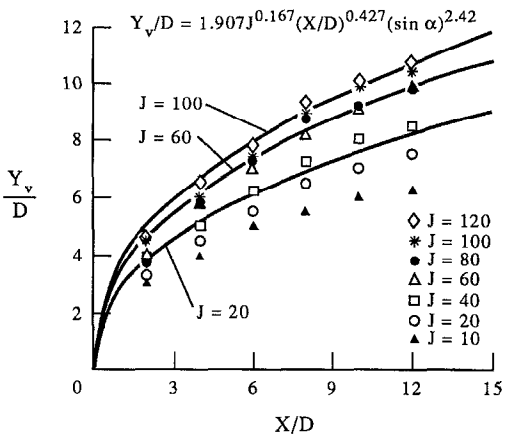

Fig. 7. Correlations of jet velocity trajectory at $\alpha = 75°$.

a given cross section, the location Y_c is the so-called *jet circulation depth*, while the location Y_v where $\tilde{U} = \tilde{U}_{max}$ is the so-called *jet velocity trajectory*. Figures 4 and 5 show that $\tilde{U}$ drops quickly above Y_v/H to a value slightly above zero, and Y_v and Y_c both increase with increasing downstream distance and incident angle.

From these velocity measurements, various dependent parameters characterizing the mixing of opposing line jets with the crossflow can be derived and correlated in terms of the independent flow and geometric variables. These include the jet velocity trajectory (or velocity penetration depth), and the length and depth of the circulation zone. After combining the data of the present work with those of Chen and Hwang [11], the correlation equations derived by the least-squares method for Y_v/D, Y_c/D, and X_R/D in terms of J, X/D, and α are summarized in Table 1. Typical correlation curves are shown in Figs. 6 and 7 for the jet velocity trajectory Y_v/D at different incident angles. Figures 6 and 7 shows that the jet velocity trajectory appears as a parabolic line ($Y_v \propto X^{0.427}$). X_R is the reattachment point that determines the length of the circulation zone. Table 1 shows that the circulation length increases with increasing momentum flux ratio and incident angle.

Typical horizontal turbulent velocity profiles are shown in Figs. 8 and 9 for $J = 100$, $\alpha = 60°$, and $J = 100$, $\alpha = 75°$, respectively. Figures 8 and 9 show that the turbulent velocity is high between Y_v and Y_c (see Figs. 4 and 5), where the mean velocity gradient is steep. However, the maximum turbulence component u'_{max} at each streamwise station X/D occurs at a location closer to the wall than the velocity trajectory Y_v. In general, the turbulence component is smaller in the channel mid-height, where the mean velocity gradient is not steep. It appears that the horizontal turbulent velocity increases slightly with increasing downstream distance.

When compared with the data of single heated line jets discharged normally into a cold crossflow ($\alpha = 90°$ in Chen and Hwang [11]), it is found that the horizontal velocity and turbulence level is higher for the opposing jets than for the one-sided jet under conditions which are otherwise the same. This is due to the fact that at $\alpha = 90°$ a local high pressure would result near the impingement point for the opposing line jets. Thus, the opposing jets will result in a higher turbulence level and better thermal mixing than the one-sided jet.

Temperature field

Typical vertical temperature profiles for various cross sections are shown in Figs. 10 and 11 for $J = 100$, $\alpha = 60°$, and $J = 100$, $\alpha = 75°$, respectively. Figures 10 and 11 also show that the temperature distribution at each cross section is almost symmetric (within the experimental uncertainty) about the channel mid-height where $Y/H = 0.5$ and $\theta = \theta^+_{min}$, and,

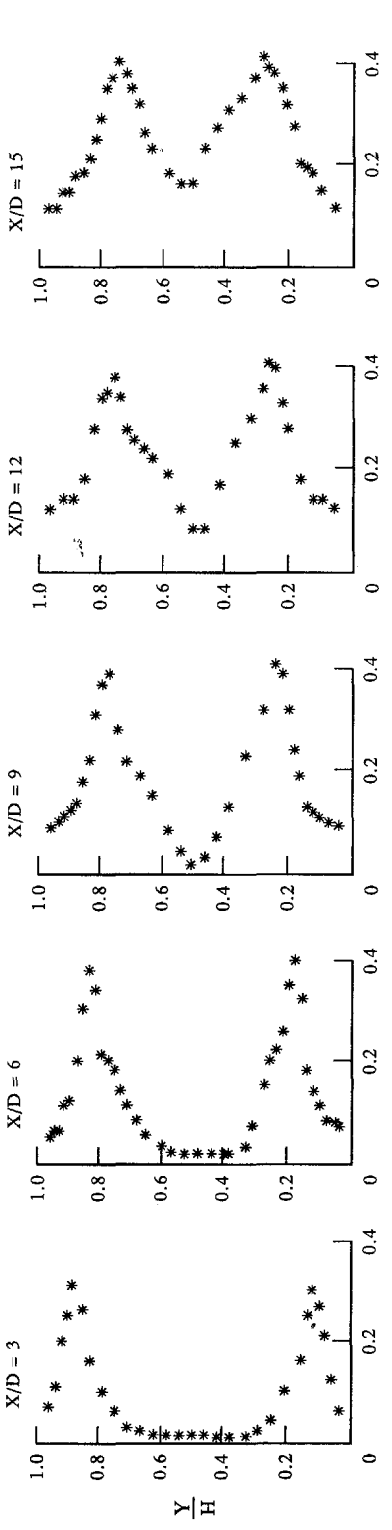

Fig. 8. Vertical turbulent velocity profiles at $J = 100$ and $\alpha = 60°$.

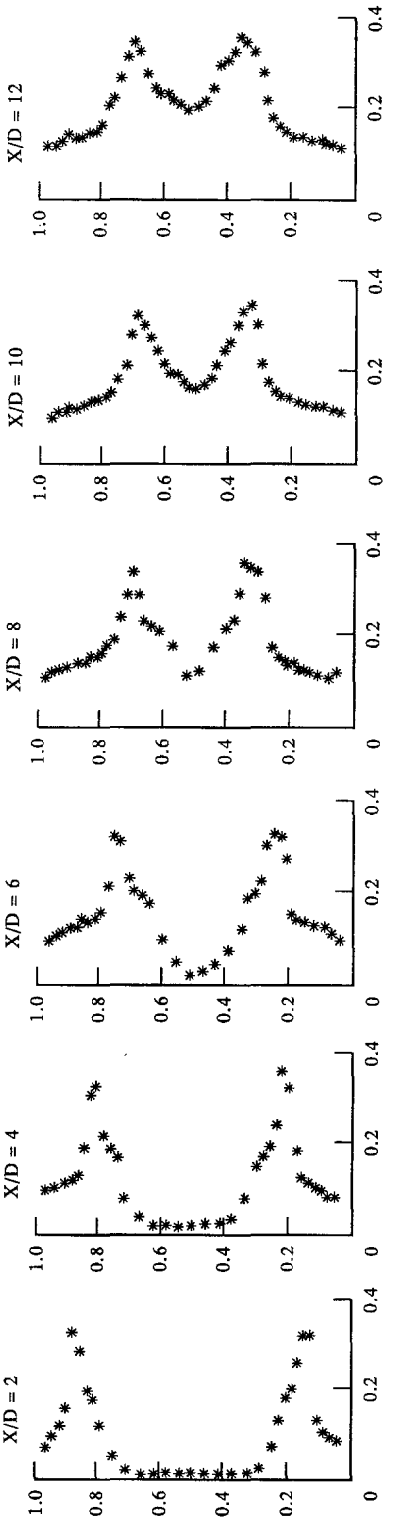

Fig. 9. Vertical turbulent velocity profiles at $J = 100$ and $\alpha = 75°$.

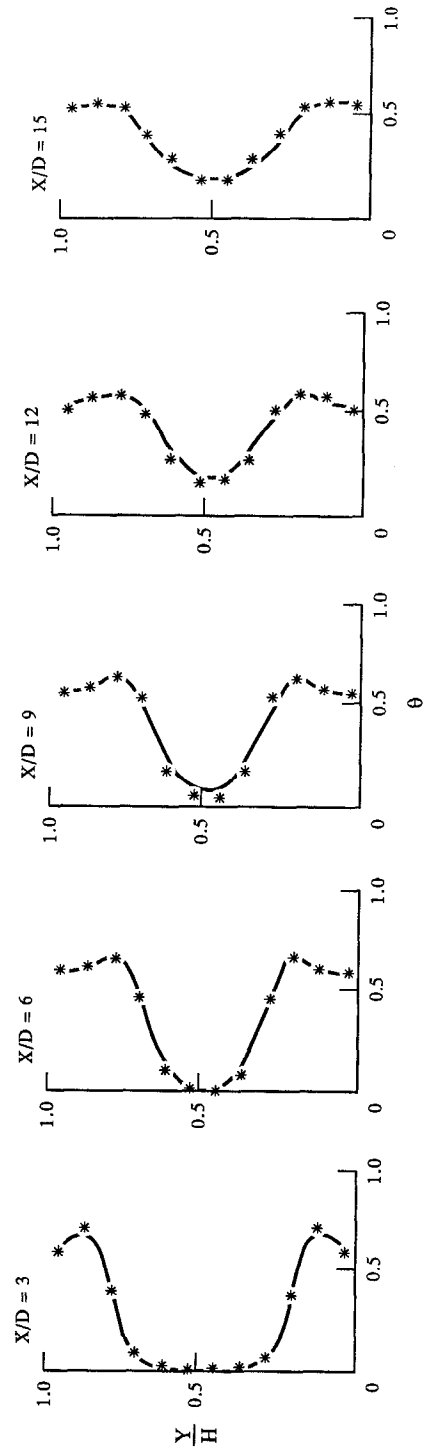

Fig. 10. Vertical temperature profiles at $J = 100$ and $\alpha = 60°$.

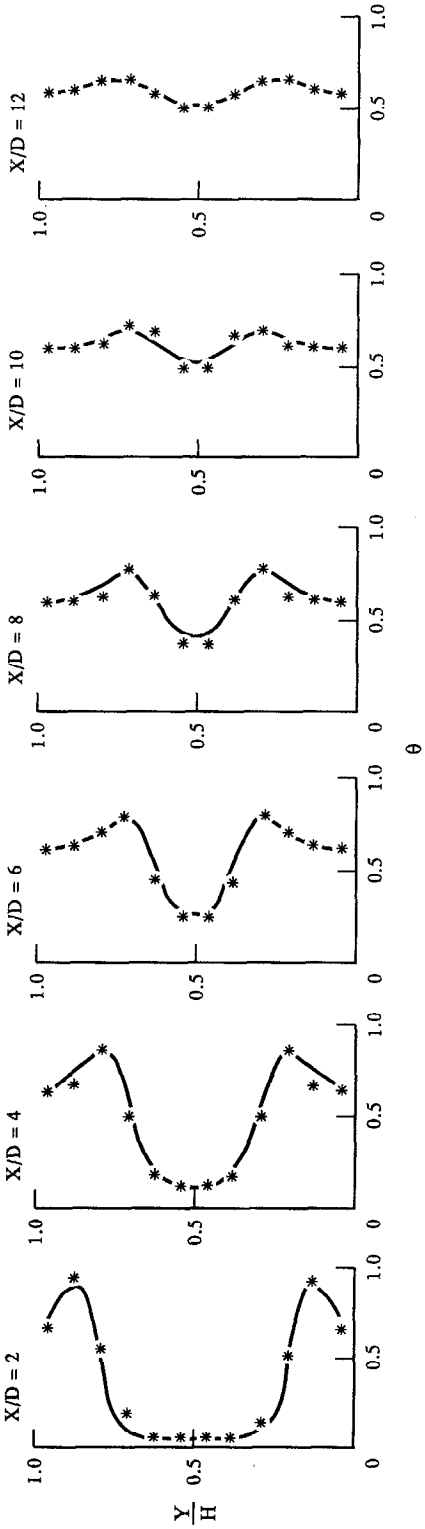

Fig. 11. Vertical temperature profiles at $J = 100$ and $\alpha = 75°$.

Table 2. Values of C_1, C_2, and C_3 in equation (3)

		C_1	C_2	C_3	α
Opposing line jets	Present work	1.067	0.54	0.45	60–90°
Single row jets	Holdeman and Walker [9]	1	ln 2	0	90°
One-sided line jets	Chen and Hwang [11]	0.573	0.215	0	90°
Opposing line jets	Chen and Hwang [11]	0.448	1.0	0	90°

thus, only the lower halves of the temperature profiles are discussed.

Figures 10 and 11 show that the temperature of the mixing air for each cross section increases from the wall with increasing height, to a maximum value θ_{max}, and decreases thereafter. The location Y_T, where $\theta = \theta_{max}$, is the so-called *thermal penetration depth* or *temperature trajectory* for a given cross section. As is shown later Y_T increases with increasing downstream distance X/D, momentum flux ratio J, and incident angle α.

Previous work by Holdeman and Walker [9] and Chen and Hwang [11] for jets discharged *normally* into the crossflow have shown the existence of local self-similar forms for the vertical temperature profiles. After combining the data of this work and Chen and Hwang [11], and taking the incident angle into account, the following self-similar forms for the vertical temperature profiles can be found:

$$\frac{\theta-\theta^{\pm}_{min}}{\theta_{max}-\theta^{\pm}_{min}} = C_1 \cdot \exp\left[-C_2\left(\frac{Y/H-Y_T/H}{W^{\pm}_{1/2}/H}\right)^2\right]\cdot(\sin\alpha)^{C_3}. \quad (3)$$

In equation (3), the constants C_1, C_2, and C_3 are determined from the data fitting, and are summarized in Table 2 for the present work and others. Equation (3) with the present findings shown in the first line of Table 2 is also expressed by the solid lines in Figs. 10–12 for different incident angles. Figures 10–12 show that the correlations fit the data fairly well. In this work, the root-mean-square deviation between the prediction by equation (3) and all data is within 11.4%. Figures 9 and 12 also show that the turbulence intensity is strong within the region of the jet half-width $W^{\pm}_{1/2}$.

From these temperature measurements, various dependent parameters characterizing the thermal mixing of opposing line jets with a crossflow can also be derived and correlated in terms of the independent flow and geometric variables. These include the jet temperature trajectory (or thermal penetration depth) Y_T, the plus- and minus-minimum temperature $\theta^{\pm}_{min}$, and the jet half-width $W^{\pm}_{1/2}$. The resulting correlation equations are summarized in Table 1. Typical correlation curves are shown in Figs. 13 and 14 for the jet temperature trajectories. Figures 13 and 14 show that the jet temperature trajectory also appears as a parabolic line ($Y_T \propto X^{0.393}$), and increases with increasing J and α. Thus, better thermal mixing can be achieved at higher jet incident angle and momentum flux ratio. The last column in Table 1 represents the root-mean-square deviation σ of the correlation from the data, and ranges from 1.76 to 24.5%.

Flow visualization

Typical flow visualization results are shown in Fig. 15(a) and (b) for $J = 100$, $\alpha = 60°$, and $J = 100$, $\alpha = 75°$, respectively. These photographs show that the velocity field is essentially symmetric about the channel mid-height. The jet velocity trajectory increases with increasing X/D to a maximum value, and decreases thereafter. Both the jet circulation depth and the circulation length increase with increasing incident angle. The LDV measurements show that the reattachment point for the case of Fig. 15(b) is $X_R/D \simeq 31.9$. All of the qualitative information depicted by the visualization results is in accordance with the measurements described previously.

CONCLUSIONS

An experimental investigation is presented for the mixing of opposing heated line jets with a cold crossflow in a rectangular channel. Measurements of the mean velocity, turbulence component, and mean temperature of the flow together with flow visualizations were made in the ranges $7.5 \leqslant J \leqslant 130$, $60° \leqslant \alpha \leqslant 90°$, and $2 \leqslant X/D \leqslant 15$ at a fixed $H/D = 24$. Correlation equations for various dependent parameters characterizing the mixing processes are given in terms of the momentum flux ratio, the downstream distance, and the incident angle.

LDV measurements show that the mixing of the opposing line jets with the crossflow would result in the circulation zones in the wall shear layers downstream of the jet openings. The turbulence level is high within the region of the jet half-width where the mean velocity gradient is steep, but the maximum value for each cross section occurs at a location closer to the channel wall than the jet velocity trajectory does. The jet velocity trajectory, and the depth and the length (or reattachment point) of the circulation zone, all increase with increasing momentum flux ratio, incident angle, and/or downstream distance.

Temperature measurements show that the vertical temperature profiles can be expressed in local self-similar forms. The jet thermal trajectory, the plus- and minus-minimum temperatures, and the jet half-widths

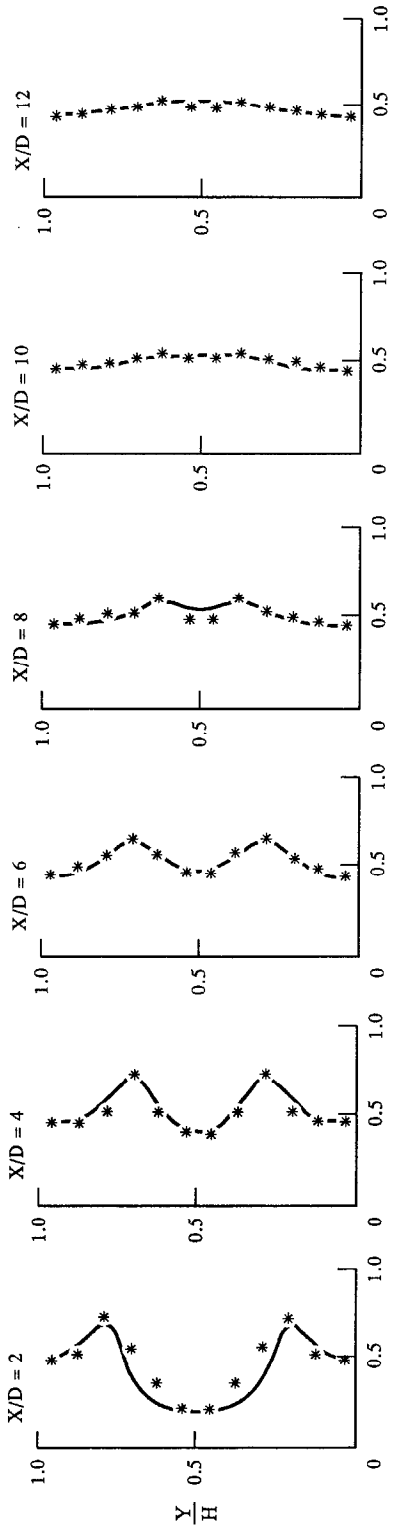

Fig. 12. Vertical temperature profiles at $J = 40$ and $\alpha = 90°$.

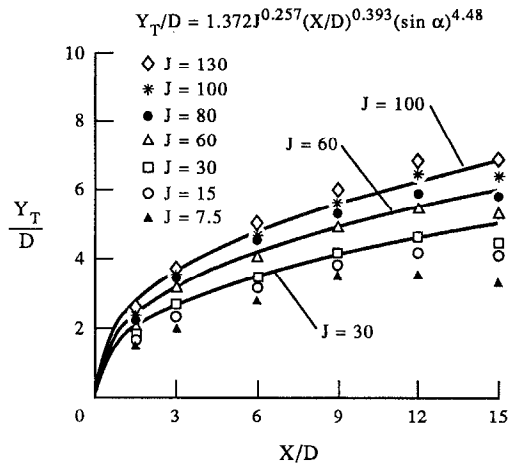

Fig. 13. Correlations of jet temperature trajectory at $\alpha = 60°$.

all increase with increasing momentum flux ratio, incident angle, and downstream distance.

When compared to the case of the one-sided jet, opposing jets will result in higher turbulence levels and better thermal mixing effects, that is, a more uniform temperature profile can be achieved in a shorter distance downstream of the jet openings by the mixing of opposing jets. This is important, for example, in the design of the dilution zone length in a gas turbine combustor, in which a more uniform temperature pattern is favored for the subsequent turbine inlet, and, thus, the size and cost of the combustion chamber can be reduced.

Acknowledgements—Partial support of this work by the National Science Council in Taiwan under Grant NSC 82-0401-E-110-034 and by the Science and Technology Coordination Council in Defense under Grant CS 79-0210-D110-03 is acknowledged.

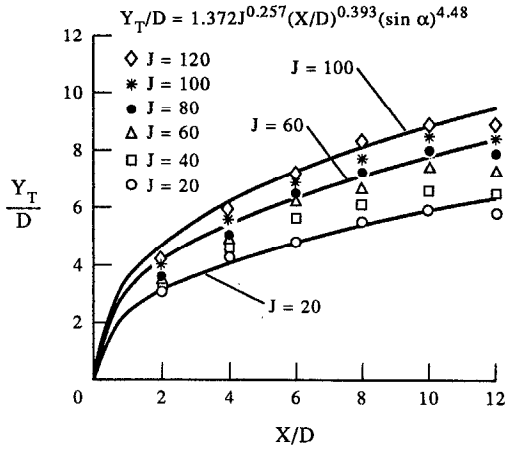

Fig. 14. Correlations of jet temperature trajectory at $\alpha = 75°$.

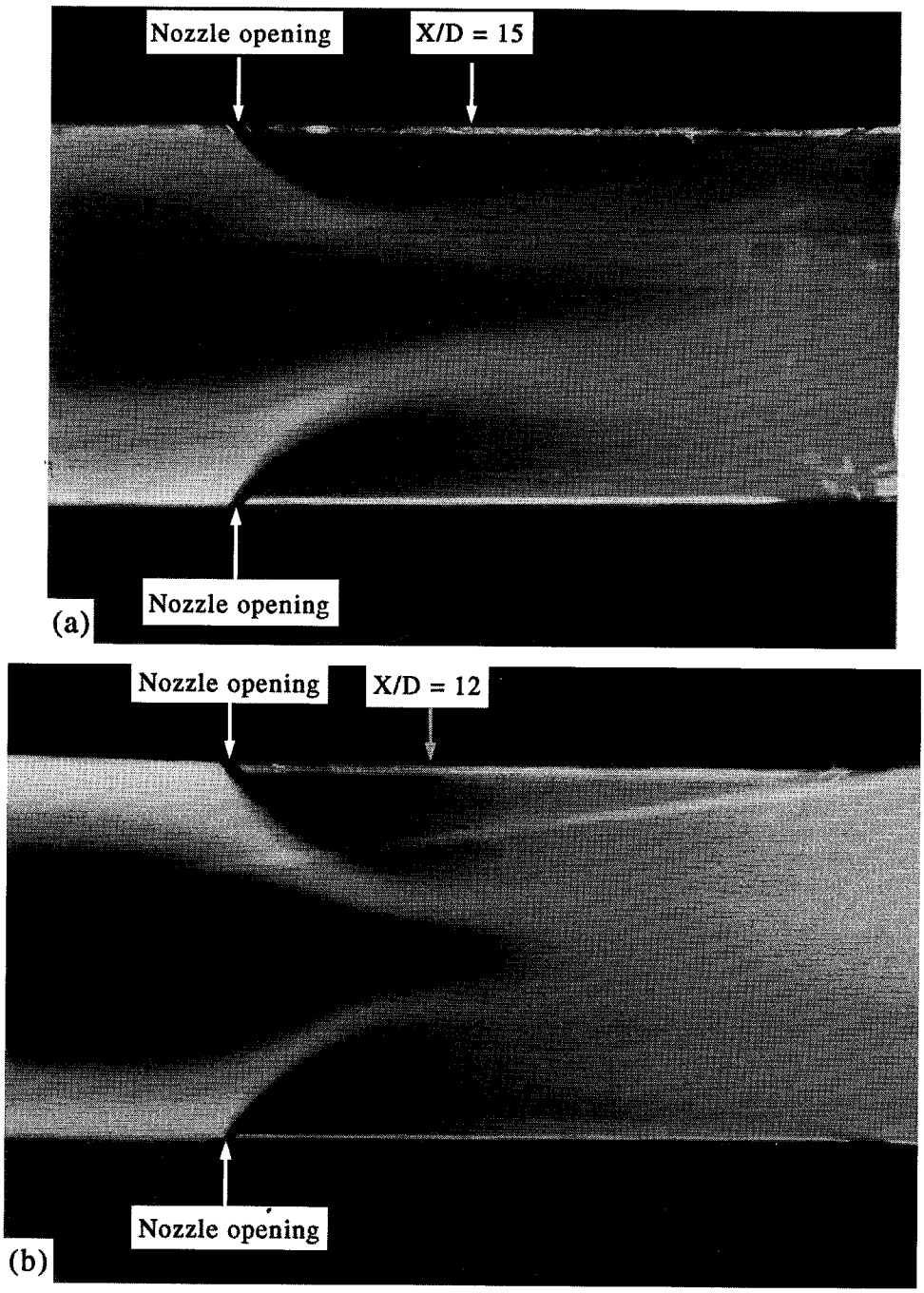

Fig. 15. Flow visualization results at: (a) $J = 100$, $\alpha = 60°$: (b) $J = 100$, $\alpha = 75°$.

REFERENCES

1. A. H. Lefebvre, *Gas Turbine Combustion*, pp. 107–137. Hemisphere, Washington, DC (1983).
2. E. E. Callagan and R. S. Ruggeri, A general correlation temperature profile downstream of a heated air jet directed perpendicular to the air stream, NACA TN-2466 (1951).
3. J. W. Ramsey and R. T. Goldstein, Interaction of a heated jet with a deflecting stream, ASME paper 71-HT-2 (1971).
4. Y. Kamotani and I. Greber, Experiments on a turbulent jets in a cross flow, *AIAA J.* **10,** 1425–1429 (1972).
5. Y. Kamotani and I. Greber, Experiments on confined turbulent jets in cross flow, NASA CR-2392 (1974).
6. J. D. Holdeman, R. E. Walker and D. L. Kors, Mixing of multiple dilution jets with a hot primary airstream for gas turbine combustors, NASA TM X-71426 (1973).
7. R. E. Walker and R. G. Eberhardt, Multiple jet study data correlations, NASA CR-134795 (1975).
8. G. B. Cox, Jr., Multiple jet correlations for gas turbine engine combustor design, *ASME J. Engng Power* **98,** 265–273 (1976).
9. J. D. Holdeman and R. E. Walker, Mixing of a row of jets with a confined crossflow, *AIAA J.* **15,** 243–249 (1977).
10. J. Andreopoulos, Measurements in jet-pipe flow issuing perpendicularly into a cross stream, *ASME J. Fluids Engng* **104,** 493–499 (1982).
11. K. S. Chen and J. Y. Hwang, Experimental study on the mixing of one- and dual-line heated jets with a cold crossflow in a confined channel, *AIAA J.* **29,** 353–360 (1991).
12. K. S. Chen and Y. R. Chang, The effects of incident angle on the mixing of opposing heated jets with a confined crossflow, National Science Council Report, NSC 82-0401-E-110-034 (1993).